Published in final edited form as:
*J Magn Reson*. 2015 January ; 250: 37–44. doi:10.1016/j.jmr.2014.10.013.

# A Cross-Polarization Based Rotating-Frame Separated-Local-Field NMR Experiment Under Ultrafast MAS Conditions

**Rongchun Zhang**[a], **Joshua Damron**[a], **Thomas Vosegaard**[b], and **Ayyalusamy Ramamoorthy**
Ayyalusamy Ramamoorthy: ramamoor@umich.edu
[a]Biophysics and Department of Chemistry, The University of Michigan, Ann Arbor, Michigan 48109-1055, United States
[b]Center for Insoluble Protein Structures (inSPIN), Interdisciplinary Nanoscience Center (iNANO) and Department of Chemistry, Aarhus University, DK-8000 Aarhus C, Denmark

## Abstract

Rotating-frame separated-local-field solid-state NMR experiments measure highly resolved heteronuclear dipolar couplings which, in turn, provide valuable interatomic distances for structural and dynamic studies of molecules in the solid-state. Though many different rotating-frame SLF sequences have been put forth, recent gains in ultrafast MAS technology have considerably simplified pulse sequence requirements due to the suppression of proton-proton dipolar interactions. In this study we revisit a simple two-dimensional $^{1}$H-$^{13}$C dipolar coupling/chemical shift correlation experiment using $^{13}$C detected Cross-Polarization with a Variable Contact time (CPVC) and systematically study the conditions for its optimal performance at 60 kHz MAS. In addition, we demonstrate the feasibility of a proton-detected version of the CPVC experiment. The theoretical analysis of the CPVC pulse sequence under different Hartmann-Hahn matching conditions confirms that it performs optimally under the ZQ ($w_{1H}$-$w_{1C}$=±$w_r$) condition for polarization transfer. The limits of the cross polarization process are explored and precisely defined as a function of offset and Hartmann-Hahn mismatch via spin dynamics simulation and experiments on a powder sample of uniformly $^{13}$C-labeled L-isoleucine. Our results show that the performance of the CPVC sequence and subsequent determination of $^{1}$H-$^{13}$C dipolar couplings are insensitive to $^{1}$H/$^{13}$C frequency offset frequency when high RF fields are used on both RF channels. Conversely, the CPVC sequence is quite sensitive to the Hartmann-Hahn mismatch, particularly for systems with weak heteronuclear dipolar couplings. We demonstrate the use of the CPVC based SLF experiment as a tool to identify different carbon groups, and hope to motivate the exploration of more sophisticated 1H detected avenues for ultrafast MAS.

### Keywords

Ultrafast MAS; Separated-Local-Field; Solid-State NMR; Cross Polarization



Correspondence to: Ayyalusamy Ramamoorthy, ramamoor@umich.edu.

## Introduction

Solid state NMR spectroscopy (ssNMR) has become a powerful tool for obtaining atomic-level structural and dynamic insight into a variety of challenging molecular systems including inorganic materials, membrane proteins, supramolecular assemblies, etc [1-4]. Separated-local-field (SLF) experiments serve as one example of the spectroscopy's powerfully informative potential as it measures heteronuclear dipolar couplings providing inter-nuclear distances along with dynamic order parameters [5-10]. SLF pulse sequences reported in the literature are generally classified as either laboratory or rotating-frame experiments. Rotating-frame techniques such as PISEMA (polarization inversion spin exchange at the magic angle) [8,11,12], HIMSELF/HERSELF (heteronuclear isotropic mixing leading to spin exchange via the local field, or heteronuclear rotating frame spin exchange via the local field) [13, 14] and their variants have been widely used in structural studies on membrane proteins and liquid crystalline materials as they provide highly resolved spectral lines in the heteronuclear dipolar coupled dimension.

In solids, the applicability of SLF techniques depends in part on the suppression of the $^{1}$H-$^{1}$H dipolar interaction (the major perpetrator to spectral resolution), which is typically accomplished by employing any combination of MAS and multiple-pulse addendums, such as Lee-Goldberg, to the SLF sequence [3, 8,11-20]. However, with the recent developments in probe technology, which have provided commercially available MAS probes capable of ∼60 kHz spinning with the fastest achieved at an impressive 110 kHz [21-31], the dominant $^{1}$H-$^{1}$H anisotropic spin interactions are largely averaged, thereby providing the desired spectral resolution and precluding the need for their RF driven suppression (beyond simple $^{1}$H decoupling during X nuclei detection, which may be achieved at significantly lower RF field strengths at ultrafast MAS[32-36]). This enables a realm of proton-detected experiments in solids, which additionally provide significant improvements in signal to noise as well as shortening experimental times [37,38]. For example, in combination with selective deuteration, ultrafast $^{1}$H NMR is already playing a significant role in the structural study of biomolecules [23,31, 38-52]. These advantages are of principal importance to proton based experiments where the requirement of small rotor volumes and sample quantity for ultrafast MAS is not a major limitation. This restriction does impose some difficulties for samples dilute in the nuclei of interest as is the case for experiments on less abundant nuclei. As a point of precautionary advise, we also mention that temperature gains can be as high as 30∼40 K for long experimental times due to spinning induced frictional heating under ultrafast spinning. This can insert some uncertainty in the accuracy of measured parameters such as dipolar coupling constants through temperature dependent dynamics along with being potentially hazardous to heat sensitive samples. Nevertheless, ultrafast MAS can be used for high throughput measurement of heteronuclear dipolar couplings using simple pulse sequences without the need for the homonuclear dipolar decoupling.

The use of ultrafast MAS was recently employed to accurately measure heteronuclear dipolar couplings with a simple $^{13}$C detected cross-polarization (CP) based rotating-frame SLF experiment [53]. This 2D ‘cross-polarization with a variable contact time’ (CPVC) SLF

experiment simultaneously increments the duration of the spin-lock RF pulses in both $^{1}H$ and $^{13}C$ RF channels to encode $^{1}H$-$^{13}C$ dipolar couplings in the second (or indirect) dimension. The aforementioned advantages for these experiments under ultrafast MAS make this a simple and elegant approach which is easy to implement. In this study we revisit this strategy by first examining the efficiency of the 2D CPVC SLF technique against Hartman-Hahn mismatch and resonance offset. Additionally, we also demonstrate a new CPVC pulse sequence with proton-detection (abbreviated as CPVC-H) under ultrafast MAS and demonstrate its unique advantage as a spectral editing tool for poorly resolved $^{1}H$ spectral lines. We hope this serves as an example to excite the community for the design of new proton-detected ultrafast techniques in light of the considerable advantages proton-detection can offer.

## Experiment and Simulation

### Materials

Uniformly $^{13}C$-labeled L-isoleucine and glycine powder samples were purchased from Cambridge Isotope Laboratory (Andover, MA), and a uniformly $^{13}C$,$^{15}N$-L-alanine was purchased from Isotec (Champaign, IL). All samples were used as received without any further purification.

### Solid-State NMR spectroscopy

All NMR experiments were performed on an Agilent VNMRS 600 MHz solid-state NMR spectrometer equipped with a 1.2 mm triple-resonance MAS probe operating at 599.8 MHz for $^{1}H$ and 150.8 MHz for $^{13}C$. All reported results were obtained at 60 kHz MAS. The sequences used for the 2D CPVC experiments are shown in Figure 1. The proton 90° pulse length was 1.2 μs for $^{13}C$-detected CPVC experiment, and 1.9 μs for the CPVC-H experiment. Proton decoupling during $^{13}C$ signal acquisition was achieved by employing the SPINAL-64 sequence [54] at an RF field strength of 45 kHz. The $^{13}C$ chemical shift was externally referenced to adamantane by setting its low-field $^{13}C$ resonance to 38.5 ppm, while the $^{1}H$ chemical shift was referenced to glycine by setting the carbonyl/amino proton signal to 8.5 ppm.

### Spin Dynamics Simulations

All numerical simulations were performed at 60 kHz MAS using the SIMPSON software [55,56]. For the $^{13}C$-detected CPVC sequence, an isolated $^{1}H$-$^{13}C$ spin pair with strong (22.3 kHz) and weak (5.0 kHz) heteronuclear dipolar couplings was used in the simulation. The $^{1}H$-$^{13}C$ dipolar splitting was obtained by directly measuring the frequency difference between the two singularities in the dipolar coupling lineshapes. For the CPVC-H sequence, we used the spin ½ nuclei in an isolated $CH_2$ group with its geometry in glycine; the $^{1}H$-$^{13}C$-$^{1}H$ angle was 109.5°. The $^{1}H$-$^{1}H$ and $^{1}H$-$^{13}C$ dipolar couplings were set at 21.0 and 22.5 kHz, respectively.

## Theoretical analysis

For simplicity, we assume an isolated $^{13}C$-$^{1}H$ pair was for our theoretical treatment. Assuming complete averaging of the $^{1}H$-$^{1}H$ dipolar coupling by ultrafast MAS, the rotating-frame Hamiltonian describing the cross polarization process under MAS is given by [57]

$$H = -w_{1I}I_x - w_{1S}S_x + 2b(t)I_zS_z - \Delta w_I I_z - \Delta w_S S_z \quad (1)$$

where $w_{1I}$ and $w_{1S}$ are the radio-frequency fields used for spin-lock on the I and S spin channels, respectively, and $\Delta w_I$ and $\Delta w_S$ are the resonance offset frequencies for I and S nuclei, respectively. The heteronuclear *IS* dipolar coupling constant *b(t)* in equation (1) is defined as

$$b(t) = -\frac{\gamma_I\gamma_S\hbar}{2r^3}\left(3\cos^2\theta(t) - 1\right) \quad (2)$$

where *r* is the internuclear distance, $\theta$ is the angle between the internuclear vector and the external magnetic field, and $\gamma_I$ and $\gamma_S$ are the gyromagnetic ratios of *I* and *S* nuclei respectively.

By defining the effective field angles as $\tan\theta_I = \frac{w_{1I}}{\Delta w_I}$, $\tan\theta_S = \frac{w_{1S}}{\Delta w_S}$, the Hamiltonian in the doubly tilted frame can be written as [57]

$$H = -w_{eI}I_z - w_{eS}S_z + 2bI_xS_x\sin\theta_I\sin\theta_S + 2bI_zS_z\cos\theta_I\cos\theta_S - 2bI_zS_x\cos\theta_I\sin\theta_S - 2bI_xS_z\sin\theta_I\cos\theta_S \quad (3)$$

Assuming a small offset frequency, that is $w_{1I} \gg |\Delta w_I|$, $w_{1S} \gg |\Delta w_S|$, $\cos\theta_I = \cos\theta_S \approx 0$; therefore, the effective Hamiltonian can be approximated as

$$H = -w_{eI}I_z - w_{eS}S_z + 2P(t)I_xS_x \quad (4)$$

with

$$w_{eI} = \sqrt{w_{1I}^2 + \Delta w_I^2},\ w_{eS} = \sqrt{w_{1S}^2 + \Delta w_S^2} \quad (5)$$

and

$$P(t) = b(t)\sin\theta_I\sin\theta_S. \quad (6)$$

According to the Hartmann-Hahn matching condition, polarization transfer occurs when $w_{eS} + \varepsilon w_{eI} \approx nw_R$ ($\varepsilon = \pm 1$, $n$=0,±1, ±2). This condition is referred to as zero-quantum (ZQ) CP when $\varepsilon = -1$ and double-quantum (DQ) CP whens $\varepsilon = +1$. The transferred CP signal at a contact time $\tau$ is given as [58]

$$S_z(\tau) = -\frac{\varepsilon\gamma_I}{2\gamma_S}\left(\frac{b_n^2}{b_n^2+\Delta\nu_n^2}\right)\left[1-\cos\left(\tau\left(b_n^2+\Delta\nu_n^2\right)^{1/2}\right)\right] \quad (7)$$

with $\Delta\nu_n = w_{1S} + w_{1I} - nw_R$.

For different matching conditions (as defined by $n$ = 0, ±1, ±2), the term $b_n$ can be written as follows:

$$b_0 = \frac{\gamma_I\gamma_S\hbar}{2r^3}\left(3\cos^2\theta(t)-1\right) \quad (8a)$$

$$b_{\pm1} = \frac{\gamma_I\gamma_S\hbar}{2\sqrt{2}r^3}\sin 2\beta \quad (8b)$$

$$b_{\pm2} = \frac{\gamma_I\gamma_S\hbar}{4r^3}\sin^2\beta \quad (8c)$$

where $\beta$ is the angle between the internuclear vector and the MAS rotor axis.

It is worth noting that the $n$=0 matching condition corresponds to the static case in the theoretical treatment presented above. Under fast MAS the $n$=0 Hartmann-Hahn matching condition, i.e. second-order CP (SOCP), can also lead to heteronuclear polarization by the second-order cross terms between homonuclear and heteronuclear dipolar couplings or the isotropic scalar (or *J)* couplings where the latter is often neglected in solids due to its relatively small magnitude [59, 60]. It should be mentioned that at least two *I* spins are necessary for this type of CP-based magnetization transfer. In an $I_2S$ spin system, the second-order cross-term between homonuclear and heteronuclear dipolar couplings can be described as:

$$H^{(2)} = w_{S1}\left(S^-I_1^+I_{2z} + S^+I_1^-I_{2z}\right) + w_{S2}\left(S^-I_2^+I_{1z} + S^+I_2^-I_{1z}\right) \quad (9)$$

where $w_{S1}$ and $w_{S2}$ are dependent on the homonuclear and heteronuclear dipolar couplings as well as the spinning rate of the sample and RF field strength [59, 60]. As such, the $n$=0 Hartmann-Hahn matching condition is not suitable for polarization transfer in this CPVC experiment, as the heteronuclear dipolar interaction during cross-polarization is also affected by the homonuclear dipolar interaction.

This theoretical approach applies to both the $^{13}$C-detected and $^{1}$H-detected CPVC experiments, as both *I* and *S* spins have identical roles during the spin-lock period. However, an important distinction arises between the two pulse sequences as we have neglected the homonuclear dipolar interaction in the beginning of the calculation [57]. Therefore, it is expected that the zero-frequency peak in the spectra obtained from the CPVC-H experiment will be much larger than that obtained using the $^{13}$C-detected CPVC experiment as $^{1}$H-$^{1}$H dipolar couplings are much larger than $^{13}$C-$^{13}$C dipolar couplings. To circumvent this

problem, we have developed a procedure for eliminating the zero-frequency peak in the heteronuclear dipolar coupling dimension of a 2D CPVC spectrum as discussed below.

Numerically simulated heteronuclear dipolar coupling spectra obtained from the CPVC method for different Hartman-Hahn matching conditions on an isolated $^{13}C$-$^{1}H$ spin pair are shown in Figure 2. A well-defined lineshape for the C-H dipolar splitting can be obtained via DQ or ZQ CP, while the dipolar splitting is completely absent under SOCP as predicted earlier. It is important to note that the DQ-CP condition requires a relatively small RF field making the associated $^{13}C$-$^{1}H$ dipolar coupling lineshape quite sensitive to $^{13}C$ resonance offset. As such, the higher RF field used in the ZQ-CP makes it a better choice for the measurement of heteronuclear dipolar couplings in the CPVC experiment.

## Treatment for eliminating the zero-frequency peak

As seen in Figure 2, a large negative zero-frequency peak exists in the *I-S* dipolar coupling spectra of ZQ or DQ CP, which can hinder the interpretation of experimental data. In practice, a special algorithm or processing method has to be applied in order to suppress the zero-frequency peak (also known as the axial peak) to obtain interpretable 2D SLF spectra. For the CPVC experiments performed on the Agilent VNMRS 600 MHz solid-state NMR spectrometer, we applied the “solvent subtraction” utility to suppress the zero-frequency peak in the *I-S* dipolar coupling dimension of the 2D spectrum. In Figure 3 we illustrate the axial peak suppression strategy for numerical simulations. First we apply a DC offset to the time-domain dipolar coupling oscillations in Figure 3(A and B). This curve is subsequently apodized as shown in Figure 3C followed by Fourier transformation. The Fourier Transformation in Figure 3 demonstrates the use of this procedure in producing the final clear lineshape as shown in the bottom right of Figure 3.

## Results and Discussion

The great advantage of the CPVC experimental approach over previous SLF experiments is the suppression of $^{1}H$-$^{1}H$ dipolar interactions by ultrafast MAS—not RF driven schemes--which considerably simplifies experimental setup in comparison to such sequences that employ, for instance, Lee-Goldberg or other homonuclear decoupling multiple pulses. The parameters for the CPVC experiment that must be carefully optimized for accurate results are the RF offset and Hartmann-Hahn matching. Herein, we systematically discuss these two experimental factors and their corresponding influence on the dipolar splittings observed in the heteronuclear dipolar coupling dimension of the 2D CPVC SLF spectrum. As both the CPVC and CPVC-H pulse sequences are exactly the same outside of the acquisition period, we limit this discussion to results from the carbon detected version.

### Resonance offset effects on CPVC performance

In rotating-frame SLF experiments like PISEMA [8, 9], dipolar splittings are quite sensitive to the 1H frequency offset which can potentially distort the accuracy of the extracted interatomic distances. This limitation is not an issue in the CPVC experiment due to the high proton RF field strength used during CP. Applied proton RF fields can be as high as 200 kHz for ultrafast MAS probes due to the utilization of micro RF coils, while the frequency

offsets are generally less than 5 kHz from the center of the proton spectrum on a 600 MHz NMR spectrometer. With these numbers in mind Eq. 5, $w_{eI}=\sqrt{w_{1I}^2+\Delta w_I^2}, w_{eS}=\sqrt{w_{1S}^2+\Delta w_S^2}$, shows that the frequency offset has a small influence on the effective RF field strength. Thus, the proton resonance offset is of little concern to the effective RF field on the proton channel. The wider chemical shift range for $^{13}$C nuclei (200 ppm corresponds to ∼30 kHz at 600 MHz) comprises a greater fraction of the applied RF field making it a legitimate concern, and necessitating the need for high $^{13}$C RF field amplitudes for uniform excitation over the entire $^{13}$C chemical shift range. Using high RF amplitudes can, however, result in RF induced heating which is undesirable for heat-sensitive samples. The balance of these restrictions for such samples makes it crucial to know the effect of $^{13}$C resonance offset on the efficiency of the CPVC SLF sequence.

As shown in Figure 4A and 4C under high RF irradiation (160 kHz and 220 kHz for $^{1}$H and $^{13}$C, respectively) the resonance offset has limited effect on the dipolar splitting;. the resonance offset only begins to have an influence when the offset frequency is greater than 15 kHz, which is generally the maximum resonance offset when the $^{13}$C carrier frequency is placed at the center of the spectrum. Therefore, as with the $^{1}$H channel, we can then safely neglect resonance offset effects at high RF fields. Outside of 15 kHz, we found that the dipolar splitting is more sensitive to the offset for a weakly $^{1}$H-$^{13}$C dipolar coupled spin system (Figure 4C) than for a strongly dipolar coupled spin system (Figure 4A). For a resonance offset of 30 kHz, the $^{1}$H-$^{13}$C dipolar splitting changes by <1 kHz for the strongly dipolar coupled spin system, while it deviates by nearly a factor of two for the weakly dipolar coupled spin system. Naturally, a high RF field strength is preferred to reduce any resonance offset effects for an accurate determination of heteronuclear dipolar couplings. To explore the effect of lower RF field strengths, we investigated the $^{1}$H-$^{13}$C dipolar splitting as a function of $^{13}$C RF field strength in Figure 4B and 4D. This was done for the same weak and strongly dipolar coupled $^{1}$H-$^{13}$C pin pair by assuming an offset of 15 kHz then simultaneously varying the $^{1}$H and $^{13}$C fields to maintain the match condition. The results clearly show that the dipolar splitting value begins to obviously deviate from the actual value when the $^{13}$C RF field amplitude is below 140 kHz. These simulated results are experimentally demonstrated in Figure 5 on a uniformly $^{13}$C-labeled isoleucine powder sample. For clarity, we only report the dipolar splitting spectral slice observed for the $CH_\alpha$ group (Figure B-E). The RF carrier frequency was set at on-resonance and 10 kHz off-resonance (below) from the $CH_\alpha$ resonance frequency. As shown in Figure 5B and 5D, when a relatively high RF field (210 kHz) was used for $^{13}$C, the resonance offset had no influence on the measured dipolar coupling value but did distort the observed lineshape. Even for an RF field as low in strength as ∼130 kHz, the observed offset (10 kHz) effect on the dipolar splitting is negligible but again results in a distorted lineshape. A $^{13}$C-$^{1}$H dipolar splitting value of ∼16.5 kHz is measured corresponding to a dipolar coupling of 23.2 kHz after taking into account the scaling factor of 0.71. Our efforts to compensate the offset dependence by using a ramped spin-lock pulse severely distorted the observed dipolar coupling lineshape shown in Figure 5E.

### Hartmann-Hahn mismatch effects on CPVC performance

The Hartmann-Hahn matching condition has a strong influence on signal sensitivity as well as the dipolar coupling scaling factor making it an important parameter for the performance of the 2D CPVC SLF experiment. As shown in Eq.(8), the heteronuclear dipolar coupling scaling factor is approximately 0.71 for the ZQ(DQ)-1 CP ($|w_{1H} \pm w_{1C}|$=60 kHz) and 0.5 for the ZQ(DQ)-2 ($|w_{1H} \pm w_{1C}|$=120 kHz) CP. As discussed above, the $^{13}$C RF amplitude during CP should be ∼140 kHz or larger to minimize any resonance offset effect. This requirement far exceeds the frequency condition for DQ-CP indicating that DQ-CP efficiency would be greatly affected by the offset frequency. As ZQ-2-CP ($|w_{1H}-w_{1C}|=2w_r$ kHz) has a smaller dipolar coupling scaling factor than the ZQ-1-CP ($|w_{1H}-w_{1C}|=w_r$ kHz), we prefer ZQ-1-CP and restrict our discussion to it. The simulated effect of the Hartmann-Hahn mismatch on the dipolar splitting is shown in Figure 6. It is clear, particularly for the weak $^{1}$H-$^{13}$C dipolar coupled system, that the dipolar splitting is quite sensitive to the Hartmann-Hahn match conditions. We compared the constant amplitude versus ramped-CP, and found that due to the high sensitivity to Hartmann-Hahn mismatch the constant-amplitude CP irradiation is preferable over the ramped-CP. While ramped-CP is often used to enhance polarization transfer, as it can restore a flat Hartmann-Hahn matching profile and overcome the effects of RF inhomogeneity and resonance frequency offset [61] its use here under ultrafast MAS—as shown in Figure 5D-- proved less effective. If employed, only a very small ramp ratio is suitable, as otherwise it will result in inaccurate dipolar splittings. The distorted result in Figure 5D, for instance, was obtained using the modest ramp ratio (defined as $(w_{highest}-w_{lowest})/(w_{highest}+w_{lowest})$) of 15%.

We mention as a practical note that the instabilities of RF power amplifier and mechanical spinning-induced heating in the probe-head can alter the RF power for the spin-locks, and therefore the Hartman-Hahn match, in the CPVC experiments [62]. To avoid these problems, we re-calibrated and optimized the RF power levels right before the start of each experiment. Nevertheless it was found that the RF power levels can fluctuate on the experimental time (about 30 min). This raises a non-trivial point to the importance and challenge of temperature control under ultrafast MAS.

In summary, the weak heteronuclear dipolar coupled spin system is more sensitive to the $^{13}$C resonance offset as well as the Hartmann-Hahn matching conditions than the strongly dipolar coupled spin system. The sensitivity of the observed dipolar splitting values to the $^{13}$C resonance offset can be generally overcome by applying high RF fields. Care should be taken when calibrating the Hartmann-Hahn match as the performance of the CPVC sequence is quite sensitive to any mismatch. We recommend a constant amplitude CP as the best choice for an efficient polarization transfer in the CPVC experiment.

### Proton-detected CPVC experiments

With the development of ultrafast MAS probe technology and the corresponding gains in spectral resolution, proton-detection is gaining more popularity within the solid-state NMR community, as it can improve the signal-to-noise of spectra as well as reduce the measurement time compared to low-γ nuclei detection [37]. Here, we propose a proton-detected CPVC pulse sequence (called CPVC-H) shown in Figure 1B, and present an

experimental demonstration on U-$^{13}$C-glycine in Figure 7. The 1D $^{1}$H spectrum under 60 kHz MAS is shown at the top of Figure 7A, where three peaks are partially resolved. Their corresponding dipolar splitting spectra are shown in Figure 7B. The peak around 8.5 ppm comprises of overlapping contributions from COOH and $NH_2$ groups. Since the $NH_2$ protons are not bonded to a carbon, in the second dimension of the CPVC-H experiment, we do not expect to see any contribution from the $NH_2$ protons. As a result, in the heteronuclear dipolar coupling dimension of the 2D CPVC-H spectrum of glycine shown in Figure 7, we observe a small $^{1}$H-$^{13}$C dipolar splitting of 2.4 kHz arising only from COOH protons, which corresponds to a $^{1}$H-$^{13}$C dipolar coupling of around 3.4 kHz after taking the scaling factor (∼0.71) into consideration. The peaks at 4.4 and 2.4 ppm correspond to the protons of the $CH_2$ group. We measured a dipolar splitting value of 16.2 kHz, corrected to 22.8 kHz after taking the scaling factor into account, which is in good agreement with previously published results [63,64]. The center peak in the dipolar splitting spectra of the $CH_2$ group may result from the slight overlap of the proton signals from COOH and $CH_2$ groups. The CPVC-H method is quite similar to the CPVC experiment proposed by Amoureux et al. [53]. Therefore, the dipolar coupling constants (and thus the bond length) measured by CPVC-H should have similar accuracies as obtained with CPVC, which, as reported by the Amoureux group, are in good agreement with X-ray diffraction analysis [53]. In Figure 7C, we demonstrate how the proton-detected CPVC experiment can be utilized to differentiate chemical groups with different $^{1}$H-$^{13}$C dipolar couplings from 1D slices extracted from the dipolar dimension.

Another experimental demonstration of the 2D CPVC-H method on a powder sample of U-$^{13}$C,$^{15}$N-L-alanine is shown in Figure 8, where obvious differences in the dipolar coupling spectra for the $CH_3$, CH and COOH groups can be observed. The rapid rotation of the $CH_3$ group averages the dipolar splitting to a relatively small value, 5.4 kHz, corresponding to a heteronuclear $^{1}$H-$^{13}$C coupling of 7.6 kHz after the scaling factor. In contrast, the CH group is quite rigid and exhibits a dipolar splitting of 15.5 kHz, corresponding to a heteronuclear $^{1}$H-$^{13}$C dipolar coupling of 21.8 kHz. This demonstrates nicely the use of the CPVC-H experiment for the dynamic studies of molecules. The measured $^{1}$H-$^{13}$C dipolar coupling value is very small for the COOH group, as the proton is not directly bonded to $^{13}$C. The wiggle in the dipolar splitting lineshape of the COOH group is an experimental artifact, which could be suppressed by increasing the number of $t_1$ experiments. Both sets of experimental results show how the proposed CPVC-H experiment is an efficient method for the measurement of heteronuclear dipolar couplings under ultrafast MAS conditions. Interestingly, a comparison of $^{1}$H detected and $^{13}$C detected experiments on U-$^{13}$C,$^{15}$N-alanine show a significant enhancement in sensitivity due to proton detection: 5.6, 4, and 6.2 for $CH_3$, CH and COOH groups.

## Conclusion

In this study, we have investigated and reported the limiting factors of a simple and robust 2D CPVC SLF pulse sequence under ultrafast MAS via numerical simulations and experiments on a uniformly-$^{13}$C-labeled isoleucine powder sample. The effects of $^{13}$C resonance offset frequency and Hartmann-Hahn mismatch were systematically analyzed for strongly and weakly heteronuclear dipolar coupled systems. A high RF field (>∼140 kHz)

on the $^{13}C$ channel is essential in overcoming the offset effects of the large spectral width of the $^{13}C$ chemical shift. Our results suggest that a constant-amplitude CP is far better than a ramp-CP for heteronuclear polarization transfer in the CPVC experiment. In addition, we have also demonstrated a proton-detected CPVC SLF experiment on U-$^{13}C$-glycine and U-$^{13}C$-$^{15}N$-L-alanine, and shown its utility as a quick and simple method for the measurement of heteronuclear dipolar couplings. We hope the proton-detected SLF experiment serves as an example of the advantages of proton detected ultrafast experiments, and excites the community for the design of additional experiments of its kind.

## Acknowledgments

This research was supported by funds from National Institutes of Health (GM084018 and GM095640 to A.R.).

## References

1. Tycko R. NMR at Low and Ultralow Temperatures. Acc Chem Res. 2013; 46:1923–1932. [PubMed: 23470028]
2. Knight MJ, Felli IC, Pierattelli R, Emsley L, Pintacuda G. Magic Angle Spinning NMR of Paramagnetic Proteins. Acc Chem Res. 2013; 46:2108–2116. [PubMed: 23506094]
3. Schmidt-Rohr, K.; Spiess, HW. Multidimensional solid-state NMR and polymers. Academic Press; 1994.
4. Ramamoorthy, A., editor. NMR spectroscopy of biological solids. CRC Press; 2010.
5. Müller L, Kumar A, Baumann T, Ernst RR. Transient Oscillations in NMR Cross-Polarization Experiments in Solids. Phys Rev Lett. 1974; 32:1402–1406.
6. Waugh JS. Uncoupling of local field spectra in nuclear magnetic resonance: determination of atomic positions in solids. Proc Natl Acad Sci USA. 1976; 73:1394–1397. [PubMed: 1064013]
7. Schmidt-Rohr K, Nanz D, Emsley L, Pines A. NMR Measurement of Resolved Heteronuclear Dipole Couplings in Liquid Crystals and Lipids. J Phys Chem. 1994; 98:6668–6670.
8. Ramamoorthy A, Wei YF, Lee Dong-Kuk. PISEMA Solid-State NMR Spectroscopy. Annu Rep NMR Spectrosc. 2004; 52:1, 52. and references cited therein.
9. Nevzorov AA, Opella SJ. Selective Averaging for High-Resolution Solid-State NMR Spectroscopy of Aligned Samples. J Magn Reson. 2007; 185:59–70. [PubMed: 17074522]
10. Bertelsen K, Paaske B, Thøgersen L, Tajkhorshid E, Schiøtt B, Skrydstrup T, Nielsen NC, Vosegaard T. Residue-Specific Information about the Dynamics of Antimicrobial Peptides from $^{1}H$-$^{15}N$ and $^{2}H$ Solid-State NMR Spectroscopy. J Am Chem Soc. 2009; 131:18335–18342. [PubMed: 19929000]
11. Wu CH, Ramamoorthy A, Opella SJ. High-resolution heteronuclear dipolar solid-state NMR spectroscopy. J Magn Reson A. 1994; 109:270–272.
12. Ramamoorthy A, Opella SJ. Two-dimensional chemical shift/heteronuclear dipolar coupling spectra obtained with polarization inversion spin exchange at the magic angle and magic-angle sample spinning (PISEMAMAS). Solid State Nucl Magn Reson. 1995; 4:387–392. [PubMed: 8581437]
13. Yamamoto K, Dvinskikh SV, Ramamoorthy A. Measurement of heteronuclear dipolar couplings using a rotating frame solid-state NMR experiment. Chem Phy Lett. 2006; 419:533–536.
14. Dvinskikh SV, Yamamoto K, Ramamoorthy A. Heteronuclear isotropic mixing separated local field NMR spectroscopy. J Chem Phys. 2006; 125:034507–034513.
15. Munowitz MG, Griffin RG, Bodenhausen G, Huang TH. Two-dimensional rotational spin-echo nuclear magnetic resonance in solids: correlation of chemical shift and dipolar interactions. J Am Chem Soc. 1981; 103:2529–2533.
16. van Rossum BJ, Ladizhansky V, Vega S, de Groot HJM. A Method for Measuring Heteronuclear ($^{1}H$-$^{13}C$) Distances in High Speed MAS NMR. J Am Chem Soc. 2000; 122:3465–3472.

17. Nevzorov AA, Opella SJ. A “Magic Sandwich” pulse sequence with reduced offset dependence for high-resolution separated local field spectroscopy. J Magn Reson. 2003; 164:182–186. [PubMed: 12932472]

18. Grinshtein J, Frydman L. Solid State Separated-Local-Field NMR Spectroscopy on Half-Integer Quadrupolar Nuclei: Principles and Applications to Borane Analysis. J Am Chem Soc. 2003; 125:7451–7460. [PubMed: 12797820]

19. Yamamoto K, Durr UHN, Xu J, Lm SC, Waskell L, Ramamoorthy A. Dynamic interaction between membrane bound full length cytochrome p450 and b5 observed by solid-state NMR spectroscopy. Scientific Reports (Nature). 2013; 3:2538.

20. Zhang R, Chen Y, Chen T, Sun PC, Li B, Ding D. Accessing Structure and Dynamics of Mobile Phase in Organic Solids by Real-Time T1C Filter PISEMA NMR Spectroscopy. J Phys Chem A. 2012; 116:979–984. [PubMed: 22185485]

21. Kobayashi T, Mao K, Paluch P, Nowak-Król A, Sniechowska J, Nishiyama Y, Gryko DT, Potrzebowski MJ, Pruski M. Study of Intermolecular Interactions in the Corrole Matrix by Solid-State NMR under 100 kHz MAS and Theoretical Calculations. Angew Chem. 2013; 125:14358–14361.

22. Parthasarathy S, Nishiyama Y, Ishii Y. Sensitivity and Resolution Enhanced Solid-State NMR for Paramagnetic Systems and Biomolecules under Very Fast Magic Angle Spinning. Acc Chem Res. 2013; 46:2127–2135. [PubMed: 23889329]

23. Nishiyama Y, Malon M, Ishii Y, Ramamoorthy A. 3D $^{15}N/^{15}N/^{1}H$ chemical shift correlation experiment utilizing an RFDR-based $^{1}H/^{1}H$ mixing period at 100 kHz MAS. J Magn Reson. 2014; 244:1–5. [PubMed: 24801998]

24. Nishiyama Y, Zhang R, Ramamoorthy A. Finite-pulse radio frequency driven recoupling with phase cycling for 2D $^{1}H/^{1}H$ correlation at ultrafast MAS frequencies. J Magn Reson. 2014; 243:25–32. [PubMed: 24713171]

25. Ye YQ, Malon M, Martineau C, Taulelle F, Nishiyama Y. Rapid measurement of multidimensional 1H solid-state NMR Spectra at ultra-fast MAS frequencies. J Magn Reson. 2014; 239:75–80. [PubMed: 24424008]

26. Bertini I, Emsley L, Felli IC, Laage S, Lesage A, Lewandowski JR, Marchetti A, Pierattelli R, Pintacuda G. High-resolution and sensitivity through-bond correlations in ultra-fast magic angle spinning (MAS) solid-state NMR. Chem Sci. 2011; 2:345–348.

27. Laage SGN, Marchetti A, Sein J, Pierattelli R, Sass HJ, Grzesiek S, Lesage A, Pintacuda G, Emsley L. Band-Selective $^{1}H$-$^{13}C$ Cross-Polarization in Fast Magic Angle Spinning Solid-State NMR Spectroscopy. J Am Chem Soc. 2008; 130:17216–17217. [PubMed: 19053413]

28. Zhang R, Ramamoorthy A. Performance of RINEPT is amplified by dipolar couplings under ultrafast MAS conditions. J Magn Reson. 2014; 243:85–92. [PubMed: 24792960]

29. Holland GP, Cherry BR, Jenkins JE, Yarger JL. Proton-detected heteronuclear single quantum correlation NMR spectroscopy in rigid solids with ultra-fast MAS. J Magn Reson. 2010; 202:64–71. [PubMed: 19857977]

30. Saalwächter K, Lange F, Matyjaszewski K, Huang CF, Graf R. BaBa-xy16: Robust and broadband homonuclear DQ recoupling for applications in rigid and soft solids up to the highest MAS frequencies. J Magn Reson. 2011; 212:204–215. [PubMed: 21803622]

31. Agarwal V, Penzel S, Szekely K, Cadalbert R, Testori E, Oss A, Past J, Samoson A, Ernst M, Böckmann A, Meier BH. De Novo 3D Structure Determination from Sub-milligram Protein Samples by Solid-State 100 kHz MAS NMR Spectroscopy. Angew Chemie Int Ed. 2014; 53:1–5.

32. Ernst M, Samoson A, Meier BH. Low-power decoupling in fast magic-angle spinning NMR. Chem Phys Lett. 2001; 348:293–302.

33. Ernst M, Samoson A, Meier BH. Low-power XiX decoupling in MAS NMR experiments. J Magn Reson. 2003; 163:332–339. [PubMed: 12914849]

34. Kotecha M, Wickramasinghe NP, Ishii Y. Efficient low-power heteronuclear decoupling in 13C high-resolution solid-state NMR under fast magic angle spinning. Magn Reson Chem. 2007; 45:S221–S230. [PubMed: 18157841]

35. Weingarth M, Bodenhausen G, Tekely P. Low-power decoupling at high spinning frequencies in high static fields. J Magn Reson. 2009; 199:238–241. [PubMed: 19467891]

36. Agarwal V, Tuherm T, Reinhold A, Past J, Samoson A, Ernst M, Meier BH. Amplitude-modulated low-power decoupling sequences for fast magic-angle spinning NMR. Chem Phys Lett. 2013; 583:1–7.
37. Paulson EK, Morcombe CR, Gaponenko V, Dancheck B, Byrd RA, Zilm KW. Sensitive High Resolution Inverse Detection NMR Spectroscopy of Proteins in the Solid State. J Am Chem Soc. 2003; 125:15831–15836. [PubMed: 14677974]
38. Marchetti A, Jehle S, Felletti M, Knight MJ, Wang Y, Xu ZQ, Park AY, Otting G, Lesage A, Emsley L, Dixon NE, Pintacuda G. Backbone Assignment of Fully Protonated Solid Proteins by 1H Detection and Ultrafast Magic-Angle-Spinning NMR Spectroscopy. Angew Chemie. 2012; 124:10914–10917.
39. Zhou DH, Shah G, Cormos M, Mullen C, Sandoz D, Rienstra CM. Proton-Detected Solid-State NMR Spectroscopy of Fully Protonated Proteins at 40 kHz Magic-Angle Spinning. J Am Chem Soc. 2007; 129:11791–11801. [PubMed: 17725352]
40. Zhou DH, Shah G, Mullen C, Sandoz D, Rienstra CM. Proton-Detected Solid-State NMR Spectroscopy of Natural-Abundance Peptide and Protein Pharmaceuticals. Angew Chem. 2009; 121:1279–1282.
41. Chevelkov V, van Rossum BJ, Castellani F, Rehbein K, Diehl A, Hohwy M, Steuernagel S, Engelke F, Oschkinat H, Reif B. $^{1}$H Detection in MAS Solid-State NMR Spectroscopy of Biomacromolecules Employing Pulsed Field Gradients for Residual Solvent Suppression. J Am Chem Soc. 2003; 125:7788–7789. [PubMed: 12822982]
42. Chevelkov V, Rehbein K, Diehl A, Reif B. Ultrahigh Resolution in Proton Solid-State NMR Spectroscopy at High Levels of Deuteration. Angew Chem Int Ed. 2006; 45:3878–3881.
43. Nishiyama Y, Endo Y, Nemoto T, Utsumi H, Yamauchi K, Hioka K, Asakura T. Very fast magic angle spinning $^{1}$H-$^{14}$N 2D solid-state NMR: Sub-micro-liter sample data collection in a few minutes. J Magn Reson. 2011; 208:44–48. [PubMed: 21035366]
44. Zhou DH, Rienstra CM. High-performance solvent suppression for proton detected solid-state NMR. J Magn Reson. 2008; 192:167–172. [PubMed: 18276175]
45. Huber M, Hiller S, Schanda P, Ernst M, Böckmann A, Verel R, Meier BH. A Proton-Detected 4D Solid-State NMR Experiment for Protein Structure Determination. ChemPhysChem. 2011; 12:915–918. [PubMed: 21442705]
46. Chevelkov V, Habenstein B, Loquet A, Giller K, Becker S, Lange A. Proton-detected MAS NMR experiments based on dipolar transfers for backbone assignment of highly deuterated proteins. J Magn Reson. 2014; 242:180–188. [PubMed: 24667274]
47. Asami S, Reif B. Proton-Detected Solid-State NMR Spectroscopy at Aliphatic Sites: Application to Crystalline Systems. Acc Chem Res. 2013; 46
48. Park SH, Yang C, Opella SJ, Mueller LJ. Resolution and measurement of heteronuclear dipolar couplings of a noncrystalline protein immobilized in a biological supramolecular assembly by proton-detected MAS solid-state NMR spectroscopy. J Magn Reson. 2013; 237:164–168. [PubMed: 24225529]
49. Zhou D, Nieuwkoop A, Berthold D, Comellas G, Sperling L, Tang M, Shah G, Brea E, Lemkau L, Rienstra C. Solid-state NMR analysis of membrane proteins and protein aggregates by proton detected spectroscopy. J Biomol NMR. 2012; 54:291–305. [PubMed: 22986689]
50. Zhou DH, Shea JJ, Nieuwkoop AJ, Franks WT, Wylie BJ, Mullen C, Sandoz D, Rienstra CM. Solid-State Protein-Structure Determination with Proton-Detected Triple-Resonance 3D Magic-Angle-Spinning NMR Spectroscopy. Angew Chem Int Ed. 2007; 46:8380–8383.
51. Bertini I, Emsley L, Lelli M, Luchinat C, Mao J, Pintacuda G. Ultrafast MAS Solid-State NMR Permits Extensive $^{13}$C and $^{1}$H Detection in Paramagnetic Metalloproteins. J Am Chem Soc. 2010; 132:5558–5559. [PubMed: 20356036]
52. Miah HK, Bennett DA, Iuga D, Titman JJ. Measuring proton shift tensors with ultrafast MAS NMR. J Magn Reson. 2013; 235:1–5. [PubMed: 23911900]
53. Paluch P, Pawlak T, Amoureux JP, Potrzebowski MJ. Simple and accurate determination of X-H distances under ultra-fast MAS NMR. J Magn Reson. 2013; 233:56–63. [PubMed: 23727588]
54. Fung BM, Khitrin AK, Ermolaev K. An Improved Broadband Decoupling Sequence for Liquid Crystals and Solids. J Magn Reson. 2000; 142:97–101. [PubMed: 10617439]

55. Bak M, Rasmussen JT, Nielsen NC. SIMPSON: A General Simulation Program for Solid-State NMR Spectroscopy. J Magn Reson. 2000; 147:296–330. [PubMed: 11097821]
56. Tošner Z, Andersen R, Stevensson B, Edén M, Nielsen NC, Vosegaard T. Computer-intensive simulation of solid-state NMR experiments using SIMPSON. J Magn Reson. 2014; 246:79–93. [PubMed: 25093693]
57. Wu XL, Zilm KW. Cross Polarization with High-Speed Magic-Angle Spinning. J Magn Reson A. 1993; 104:154–165.
58. Amoureux JP, Pruski M. Theoretical and experimental assessment of single- and multiple-quantum cross-polarization in solid state NMR. Mol Phys. 2002; 100:1595–1613.
59. Lange A, Scholz I, Manolikas T, Ernst M, Meier BH. Low-power cross polarization in fast magic-angle spinning NMR experiments. Chem Phys Lett. 2009; 468:100–105.
60. Scholz I, Meier BH, Ernst M. Operator-based triple-mode Floquet theory in solid-state NMR. J Chem Phys. 2007; 127:204504. [PubMed: 18052439]
61. Metz G, Wu XL, Smith SO. Ramped-Amplitude Cross Polarization in Magic-Angle-Spinning NMR. J Magn Reson A. 1994; 110:219–227.
62. Langer B, Schnell I, Spiess HW, Grimmer AR. Temperature Calibration under Ultrafast MAS Conditions. J Magn Reson A. 1999; 138:182–186.
63. Dvinskikh SV, Zimmermann H, Maliniak A, Sandstrom D. Heteronuclear dipolar recoupling in liquid crystals and solids by PISEMA-type pulse sequences. J Magn Reson. 2003; 164:165–170. [PubMed: 12932469]
64. Zhao X, Edén M, Levitt MH. Recoupling of heteronuclear dipolar interactions in solid-state NMR using symmetry-based pulse sequences. Chem Phys Lett. 2001; 342:353–361.

## Highlights

- A $^{1}$H-evolved, $^{1}$H-detected rotating-frame SLF is demonstrated under ultrafast MAS.
- CP-based SLF sequence is quite sensitive to Hartmann-Hahn mismatch.
- CP-based SLF sequence is insensitive to offset when high RF fields are used.
- A constant-amplitude-CP SLF renders a better performance than a ramped-CP SLF.
- $^{1}$H-detection greatly enhances the sensitivity of CP-based rotating-frame SLF.

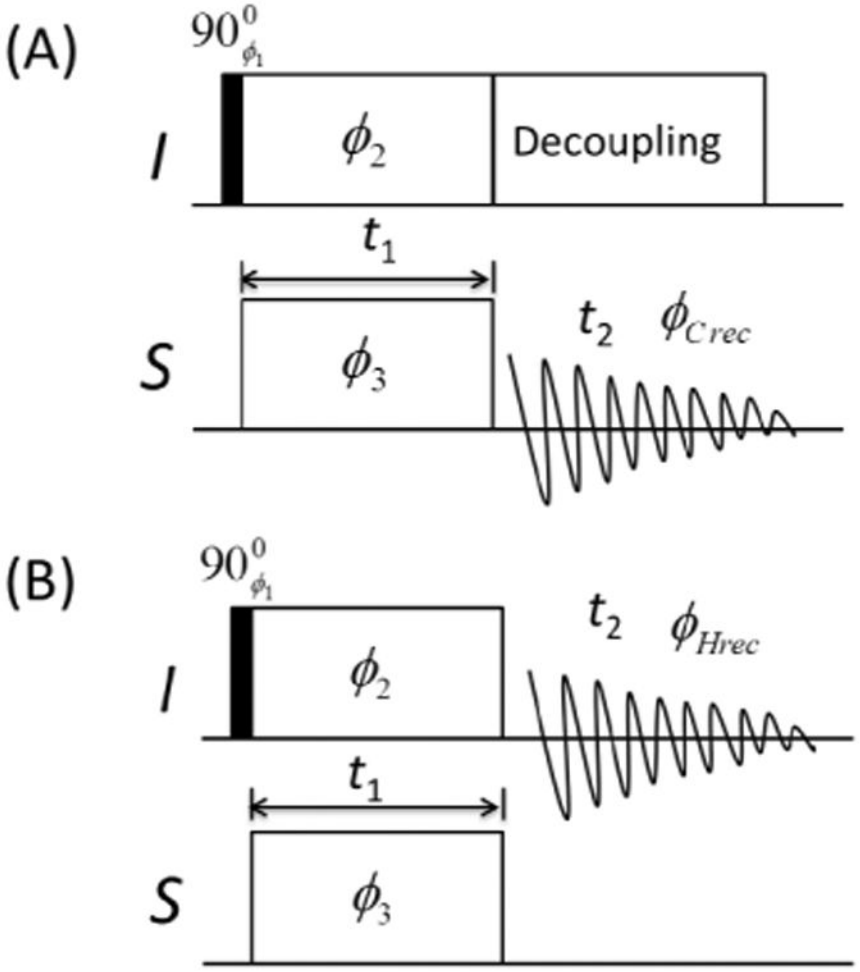


**Figure 1.**

Schematics of radio-frequency pulse sequences used in this study for $^{13}$C-detected (A) and $^{1}$H-detected (B) cross-polarization with a variable contact time (CPVC) 2D SLF experiment. The $t_1$ incrementation was achieved by simultaneously increasing the spin-lock durations in the cross-polarization sequence. SPINAL-64 was used to decouple protons during signal acquisition for the $^{13}$C-detected CPVC experiment. The following phase cyclings were used in the experiment: $\varphi_1$=0,2,0,2; $\varphi_2$=1,1,1,1; $\varphi_3$=0,0,1,1; $\varphi_{Crec}$=0,2,1,3; $\varphi_{Hrec}$=0,2,0,2.

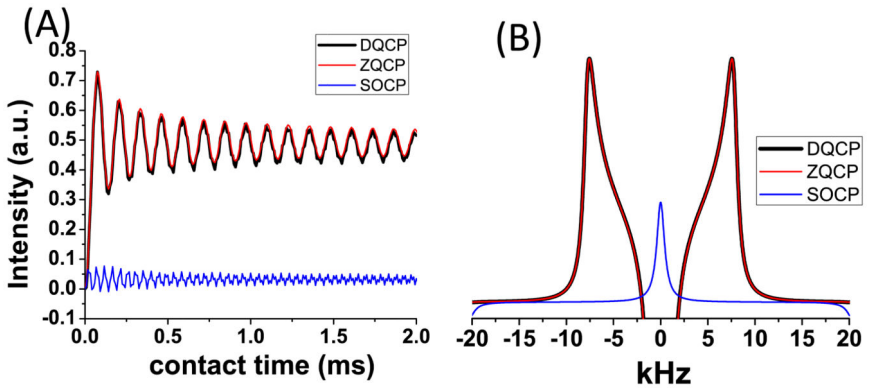


**Figure 2.**

Simulated time dependence of I-S dipolar coupling (A) and dipolar splitting spectra (B) for ZQ CP with $w_{1H}$=160 kHz and $w_{1C}$=220kHz, DQ CP with $w_{1H}$=20kHz and $w_{1C}$=40 kHz, and SOCP with $w_{1H}$= $w_{1C}$=40 kHz. Results show superior performances of DQ and ZQ CP sequences and the inefficiency of SOCP sequence. ZQCP is recommended due to other advantages as mentioned in the main text.

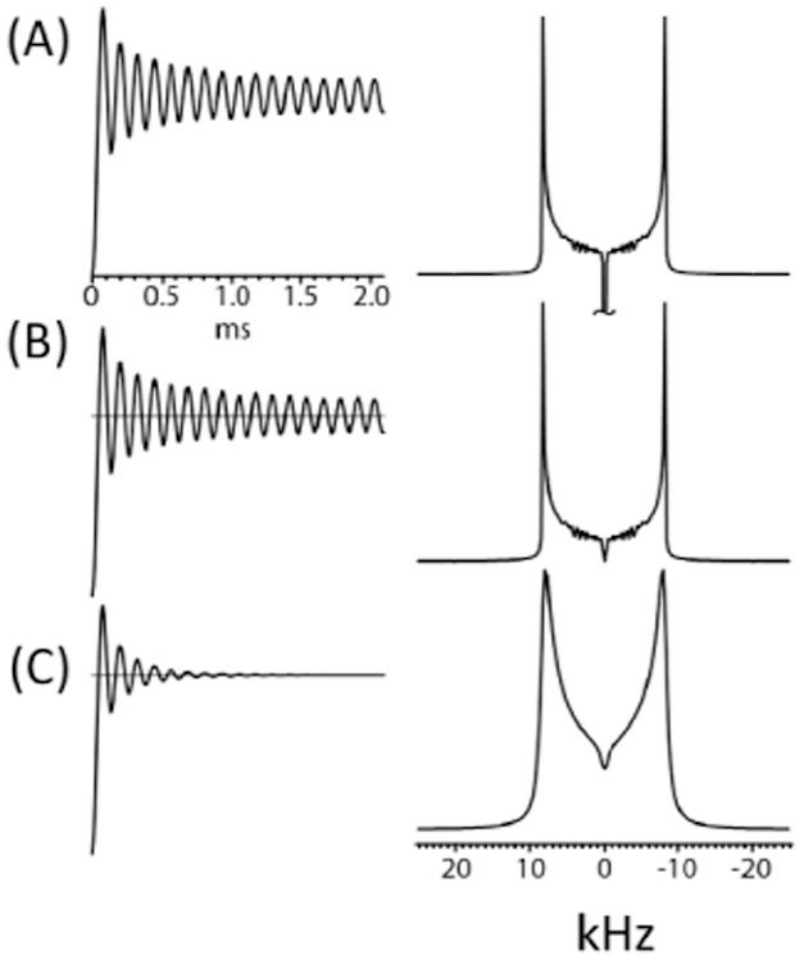


**Figure 3.**

A simple data processing procedure to surpress axial peaks in 2D CPVC SLF spectra. Time-domain signals (left) and corresponding Fourier-transformed frequency spectra (right). (A) An oscillating buildup curve from CPVC before (A) and after compensation for the DC offset without (B) and with (C) apodization.

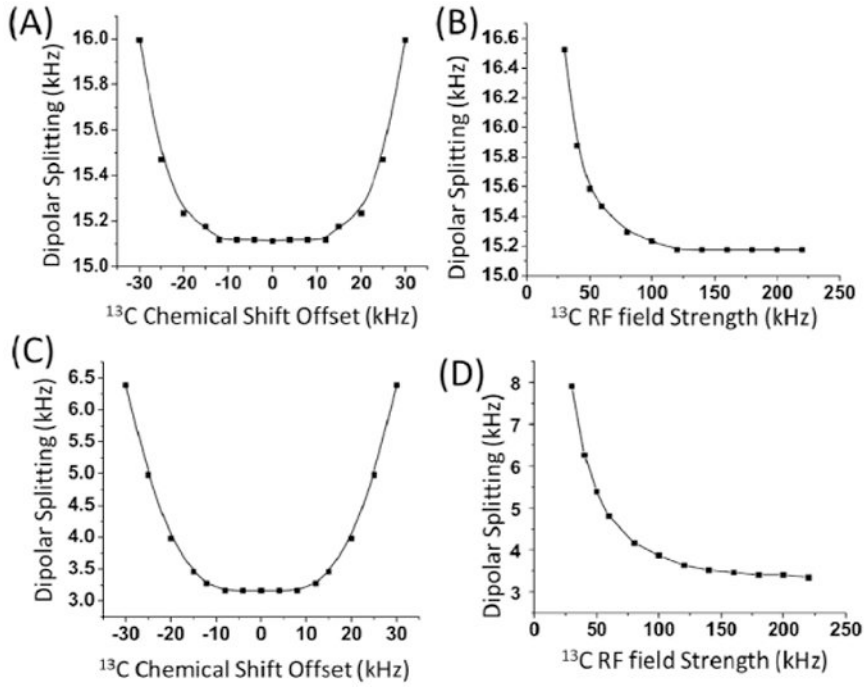


**Figure 4.**

Simulated dipolar splitting as a function of (A and C) $^{13}C$ resonance offset and (B and D) $^{13}C$ RF field amplitude during the cross-polarization process for an isolated $^{13}C$-$^{1}H$ spin pair with a heteronuclear coupling of 22.3 kHz (A and B) or 5 kHz (C and D). For (A, C), the RF field amplitudes used were 160 kHz and 220 kHz on the proton and carbon channels, respectively. For (B,D), the $^{13}C$ frequency offset was set at 15 kHz and the $^{1}H$ field amplitude was varied with the $^{13}C$ field amplitude so that $w_{1H}$-$w_{1C}$=60 kHz when $w_{1C}$ 160 kHz and $w_{1C}$-$w_{1H}$=60 kHz when $w_{1C}$ 160 kHz.

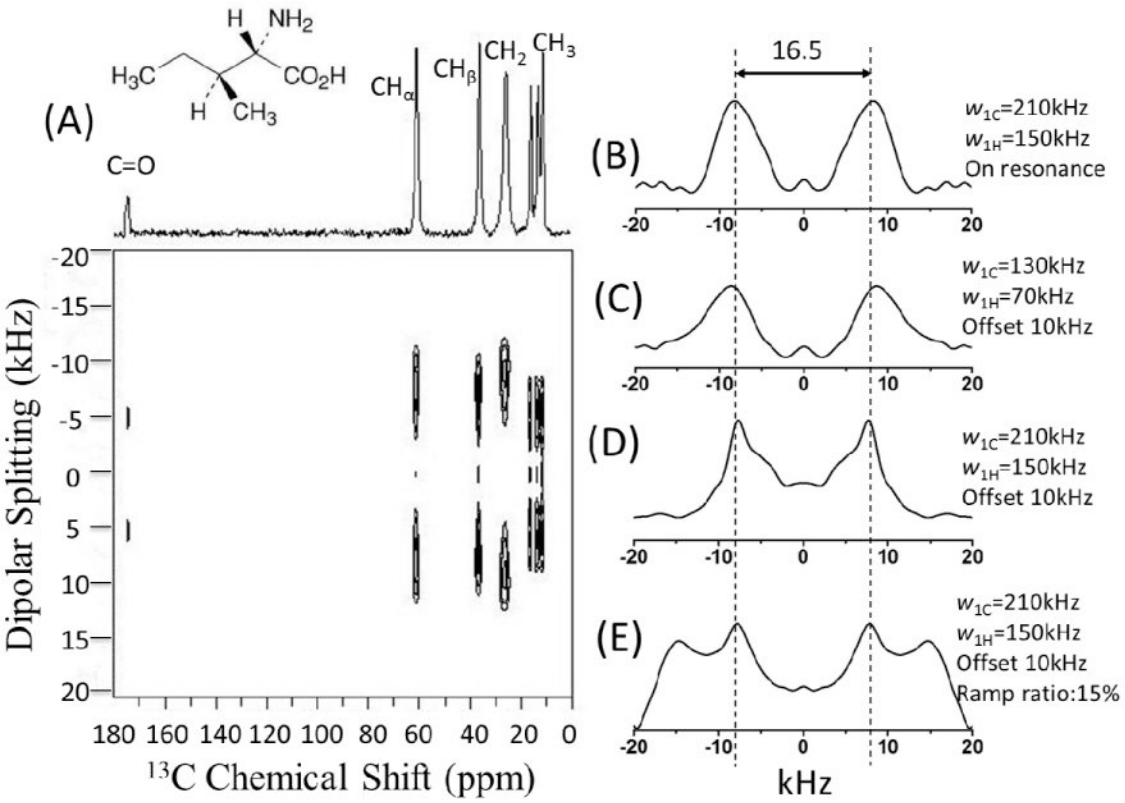


**Figure 5.**

(A) $^{13}$C-detected 2D CPVC SLF spectrum of a uniformly-$^{13}$C-labelled isoleucine powder sample obtained at 60 kHz MAS. $^{1}$H-$^{13}$C dipolar splitting spectra for the $CH_{\alpha}$ group extracted from 2D CPVC SLF spectra obtained under various conditions: with the $^{13}$C carrier frequency set at the $^{13}C_{c}$ resonance position (B) and 10 kHz offset below the $^{13}C_{\alpha}$resonance frequency (C, D, E). For (B, C, D), constant amplitude spin-locks were used for Hartmann-Hahn CP, while for (E) a ramped-CP was used with a 15% ramp size on the $^{13}$C spin-lock. For the ramped-CP, the ramp ratio is defined as $(w_{highest}-w_{lowest})/(w_{highest}+w_{lowest})$.

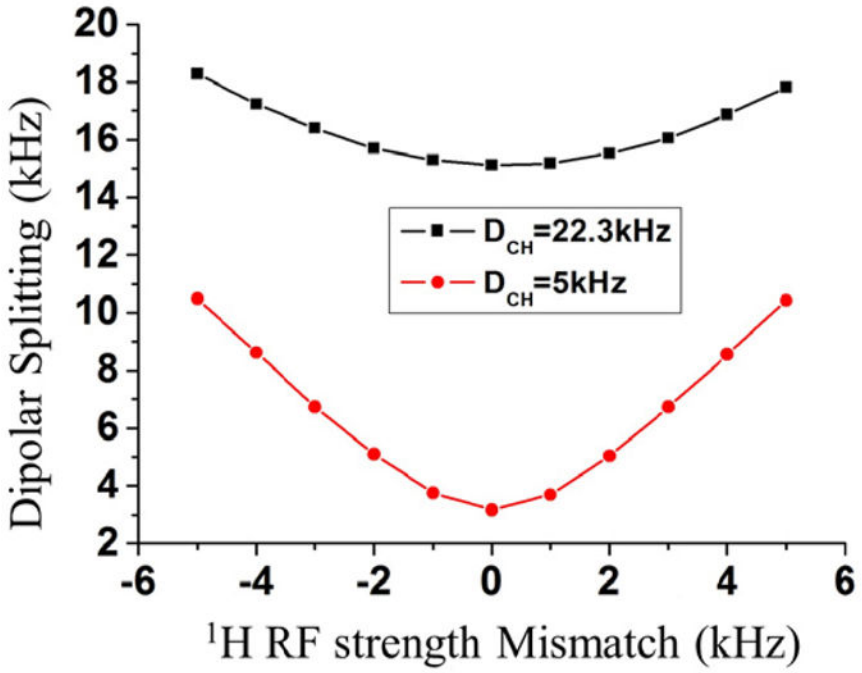


**Figure 6.**

Simulated dipolar splitting as a function of Hartman-Hahn mismatch $^1$H RF amplitude during the CP process for an isolated $^{13}$C-$^1$H spin pair with strong or weak heteronuclear dipolar couplings. During cross polarization, the $^{13}$C RF amplitude was set at 220 kHz, while it is 160 kHz on the $^1$H channel when the mismatch was zero.

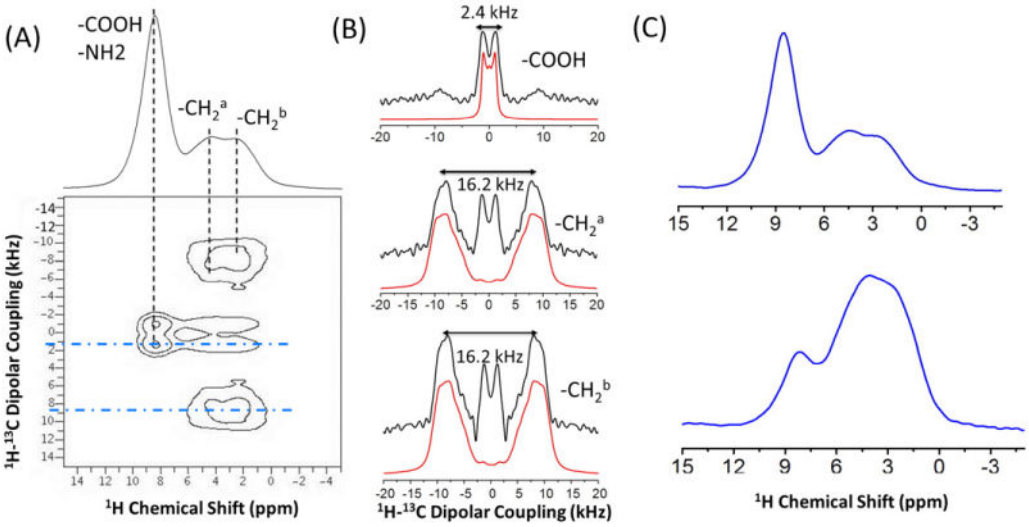


**Figure 7.**

(A) The $^{1}$H-detected 2D CPVC SLF spectrum of U-$^{13}$C-glycine powder sample with the $^{1}$H chemical spectrum shown at the top. (B) $^{1}$H-$^{13}$C dipolar splitting spectral slices extracted along the F1 dimension at different $^{1}$H chemical shifts corresponding to the black dashed lines in (A). Simulated spectra are shown in red and experimental in black. The line broadening used for the simulation of the dipolar splitting spectra of COOH and $CH_2$ groups are 500 and 1500 Hz, respectively. (C) $^{1}$H spectral slices extracted along points in the dipolar coupling dimension which correspond to the blue (dot-dash) lines of the 2D spectrum in (A).

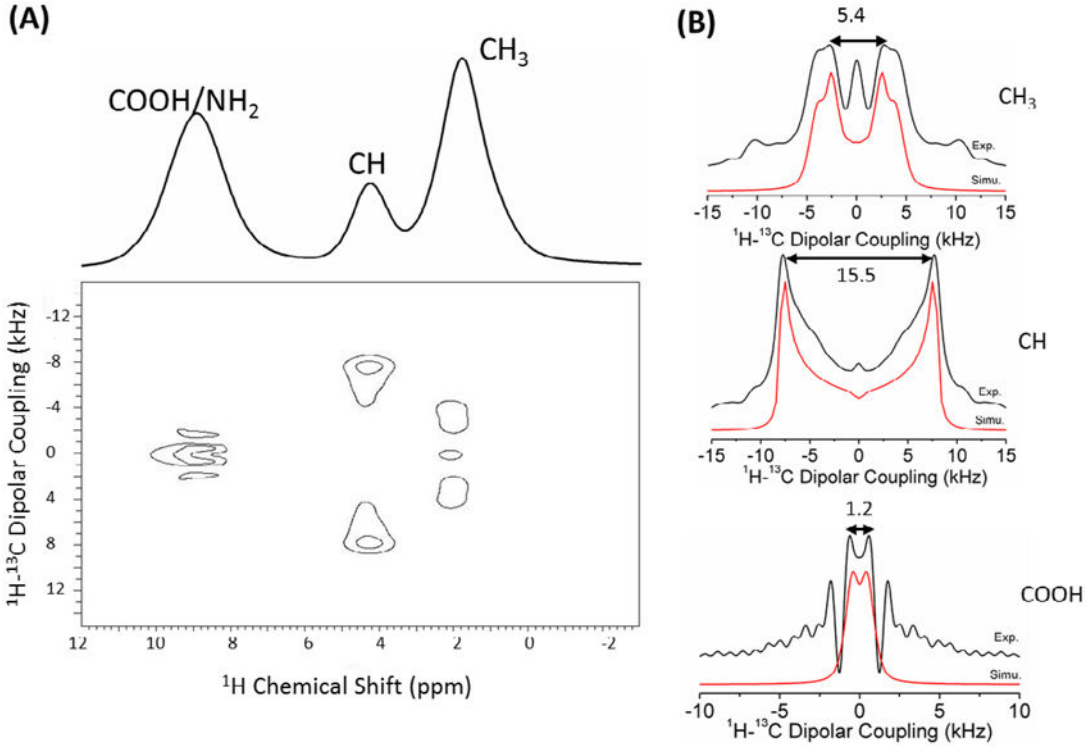


**Figure 8.**

(A) The $^{1}$H-detected 2D CPVC SLF spectrum of a powder sample of U-$^{13}$C-$^{15}$N-L-alanine with the $^{1}$H spectrum shown at the top. (B) $^{1}$H-$^{13}$C dipolar splitting spectral slices extracted along the dipolar coupling dimension at different $^{1}$H chemical shift values. Simulated (red) and experimental (black) spectra are compared. The line broadening factors used in the simulation of the dipolar splitting spectra of $CH_3$, CH, and COOH groups are 900, 300 and 1000 Hz, respectively. 32 $t_1$ increments were used for encoding heteronuclear dipolar couplings.